2026 IEEE International Conference on Robotics and Automation (ICRA 2026)
June 1-5, 2026. Vienna, Austria

Estimating Force Interactions of Deformable Linear Objects from their Shapes

Qi Jing Chen[1], Shilin Shan[1], Timothy Bretl[2], and Quang-Cuong Pham[3]

***Abstract*— This work introduces an analytical approach for detecting and estimating external forces acting on deformable linear objects (DLOs) using only their observed shapes. In many robot-wire interaction tasks, contact occurs not at the end-effector but at other points along the robot's body. Such scenarios arise when robots manipulate wires indirectly (e.g., by nudging) or when wires act as passive obstacles in the environment. Accurately identifying these interactions is crucial for safe and efficient trajectory planning, helping to prevent wire damage, avoid restricted robot motions, and mitigate potential hazards. Existing approaches often rely on expensive external force-torque sensors or that contacts occur at the end-effector for accurate force estimation. Using wire shape information acquired from a depth camera and under the assumption that the wire is in or near its static equilibrium, our method estimates both the location and magnitude of external forces without additional prior knowledge. This is achieved by exploiting derived consistency conditions and solving a system of linear equations based on force-torque balance along the wire. The approach was validated through simulation, where it achieved high accuracy, and through real-world experiments, where accurate estimation was demonstrated in selected interaction scenarios.**

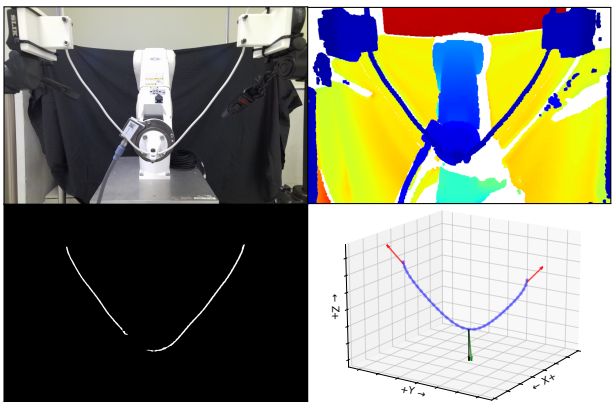

Fig. 1. Overall Force Estimation Process. Rowwise from top left to bottom right: Real image of experiment, depth information, segmentation mask of wire, and final smoothed wire shape with actual and estimated forces (arrows: red - estimated end-clamp force, black - actual force, green - estimated external force).

I. Introduction

Force feedback of robotic interaction with wires can be useful for trajectory planning or implementing safety conditions during collisions [1]–[5]. In many such scenarios, the robot does not directly grasp or manipulate the wire – for example, when a robotic arm nudges a wire into place. In other cases, wires serve merely as passive elements or environmental obstacles that the robot must navigate around. A clear example of these cases can be found in car manufacturing plants [6] and medical suturing applications [7]. For the case of a robot arm, a common robotic manipulator for wires, force sensors are generally mounted on the end-effector. This allows for interaction forces of an end-effector gripper with a wire to be easily recorded. The problem arises when robot-wire interactions do not happen at the end-effector but instead at other locations along the robot arm. These interactions must be considered because they could lead to restricted or potentially dangerous movement of the robot. Too much tension in the wires could lead to breakages of the wires in the environment. If it is not the wire that breaks, the robot arm could become caught and generate excessive torque, leading to both safety hazards and potential motor damage. Understanding these interaction forces will allow robots to plan their trajectory based on expectations of how a wire would react to its immediate movement.

For this reason, we introduce an algorithm which estimates the forces on a wire based on its shape. From here we will refer to the wire as an elastic rod. Our work derives consistency conditions, based on force torque balance equations, which determine if sections of an elastic rod in static equilibrium belong to the same undisturbed section where no external interaction forces are present between them. With the section classification and knowledge on the internal stiffness torques of the elastic rod based on the discrete elastic rods (DER) model [8], directions and magnitudes of external forces on the rod can be solved for. Due to the indeterminate nature of the problem (explained in Section IV-B.2), the algorithm proceeds by either assuming zero external torque and solving for the force positions, or by assuming that forces are applied at the midpoint of each section and solving for the resulting external torque. A solution to obtain both torques applied and force positions is by detecting collision points along the wire in the real image and identifying their positions visually, although this method will not be discussed in our work. We observe that our approach is closely related to existing proprioceptive sensor-based force and collision estimators [9]–[11]. However, prior work primarily applies these methods to robotic arms, where accurately localizing contact forces and estimating their magnitudes remains challenging. In contrast, our method transfers this idea to the wire, leveraging the internal torques of an elastic rod as a proxy for proprioceptive sensing within a similar estimation framework. The inherent

*Github repo: `https://github.com/qj25/ds2f` (Videos: `https://youtu.be/fAAVQuVog4Y`)

[1]Nanyang Technological University, School of Mechanical and Aerospace Engineering, [2]University of Illinois Urbana-Champaign, [3]Eureka Robotics, Singapore

discretization of the wire allows for more accurate force localization and estimation.

Contributions of the paper

The contributions of this paper are twofold. First, we formulate a set of novel consistency conditions to estimate the positions of external interactions along an elastic rod in static equilibrium (Section IV-A). Prerequisite assumptions are also stated to ensure the problem is not underdetermined.

Second, using the positions of interactions, parameters of the force and torque can be solved for using a system of linear equations derived from the force-torque balance in each discretized rod piece (Section IV-B). Due to the nature of the problem, one can either solve for the external torque applied or the exact positions of force application, the former requiring an assumption of force application being at the center of mass of the discrete piece, and the latter with the assumption that there is no external torque applied at that discrete piece.

II. Related Works

Robotic manipulation of Deformable Linear Objects (DLOs) increasingly emphasizes force sensing and control to overcome limitations such as unknown object properties and visual occlusions. Robots operating in complex or unstructured environments require sophisticated capabilities to safely interact with their surroundings, particularly concerning detecting physical contact and understanding interaction forces.

A. Force Control for DLO Manipulation

Foundational work investigated characteristics in force signals for detecting contact state transitions between a DLO and rigid obstacles [1]. Research reveals that the set of all static equilibrium configurations for a Kirchhoff elastic rod constitutes a smooth manifold of finite dimension that can be explicitly parameterized by moments and forces at the elastic rod base [12], and its free configuration space is path-connected [13]. This significantly simplifies and enables the construction of gripper paths for manipulation planning of DLOs. Complementary methods focus on estimating DLO shape or contact information primarily from force/torque sensing, achieving real-time 3D shape estimation of elastic rods via a discretized Kirchhoff elastic rod model with gravity compensation [3], [14], or by keeping the DLO under tension for contact inference and primitive execution [4]. Another method is to learn force-based manipulation skills from demonstrations for variable-impedance control, enabling tasks like knot-tightening despite challenges in capturing accurate force profiles [2].

B. Contact Detection and Force Estimation

External tactile sensors can detect contact directly but are expensive to integrate [15]–[17]. To that end, it was found that proprioceptive sensors of the robot can be used for contact detection [18]–[20]. Two main issues faced when using proprioceptive sensors to detect collisions are the system dynamic modeling inaccuracies and the noise from proprioceptive sensors [21]. These problems affect the accuracy of the estimated external joint torques and could lead to false positives in contact detection.

Simpler robot models are generally successful in force estimation [22], some integrating visual information as a tool [23]. Difficulties in modeling the non-linear dynamics of the whole robot arm has led to the utilization of a model-based Kalman filters with motor signals [9], an Extended Kalman Filter torque fusion method [10], and a model-free learning-based neural network approach [11]. Such methods require accurate calibration in the event of modifications to the robot structure which affect its dynamics [24], [25]. Although these works showed some success in estimating the direction, magnitude, and position of external forces, they require additional assumptions such as having only one external contact point [26], or that the contacts are applied sequentially [27], due to the underdetermined nature of the problem. The handling of numerous contacts is still a problem that demands attention. This idea of contact detectability has been discussed in-depth [28], in which small motions that most effectively falsify spurious contact positions have been found. Vision and depth sensing has been utilized in a GPU parallel processing algorithm to effectively determine contact points on a robot arm and react accordingly [29].

Prior work on shape-based force estimation spans simplified, numerical, and probabilistic formulations. Planar Cosserat rod models have enabled real-time tip force estimation without physical sensors, though restricted to 2D settings [30]. Constrained nonlinear optimization has been used to fit large-deflection 3D Cosserat models to observed shapes, though experimental validation was primarily planar [31]. Gaussian-parameterized, EKF-based formulations later enabled simultaneous estimation of distributed load magnitude and location under sparse sensing, at the cost of manual noise tuning and increased computational latency [32]. Probabilistic continuous-time Gaussian process methods have also been proposed for joint or force-independent backbone estimation [33], [34]. While these numerical approaches provide flexibility and uncertainty modeling, they generally require hyperparameter tuning and iterative solvers, motivating the deterministic analytical formulation adopted in this thesis.

III. Problem Definition

In the following, we use the terms ‘elastic rod’ and ‘wire’ interchangeably. We define a rod piece as a discrete section between consecutive nodes of a discretized rod. A section is then defined as a set of consecutive rod pieces that share one or more properties. We classify pieces of a discretized elastic rod into two section types (s-types): Undisturbed (UD) and Disturbed (D). A UD section is defined as a set of consecutive discretized rod pieces to which no external disturbances are applied. A D section is defined as a set that has at least one disturbance applied to one or more of its pieces. An elastic rod is discretized into $n = n_{\text{UD}} + n_{\text{D}}$ pieces where $n_{\text{s-type}}$ is the total number of s-type pieces (s-type being either UD or D). $N = N_{\text{UD}} + N_{\text{D}}$ is the total number of sections and $N_{\text{s-type}}$ is the number of s-type sections. Each

piece edge in the discretized rod is defined as $\mathbf{e}^i = \mathbf{x}_{i+1} - \mathbf{x}_i$ where $\mathbf{x}_i$ is the Cartesian position of the $i-$th node. Each D_j (the j^{th} D section) has a set of external force-torque, $\{\mathbf{f}^j, \tau^j\}$, where $0 \leq j < N_\mathrm{D}$. Theoretically, our method should be able to detect all force disturbances on an elastic rod provided it fulfills the following condition:

- **Quasistatic motion**: Elastic rod must be in static equilibrium or quasistatic motion. This forms the basis of our method and allows us to derive the equations required.
- **Cardinality**: Rod must be sufficiently discretized. For UD_j, the number of pieces is such that $N_{\mathrm{UD}_j} \geq 3$. This ensures that a necessary and sufficient condition can be formed to classify pieces.
- **Non-collinearity**: Letting $\mathbf{UD}_j = \{\mathbf{v}_1, \mathbf{v}_2, \ldots, \mathbf{v}_n\}$ be the vectors of the UD pieces, there exist distinct vectors $\mathbf{v}_i, \mathbf{v}_j, \mathbf{v}_k \in \mathbf{V}$ such that no two are parallel. This ensures the problem is not underdetermined. To provide an intuitive example: shape of a completely taut wire does not visibly change in response to variations in external force, making it impossible to visually infer the exact force magnitude (assuming negligible axial stretching).
- **Perfect elasticity**: Rod behavior closely follows the elastic rod theory used. This ensures that the classification and force estimation is accurate.

While our proposed method is tested with straight isotropic rods for implementation simplicity, the pipeline is rod-model independent and can handle both bent and anisotropic rods. Axial stretching of the wire is assumed to be negligible, which is typically the case for most robot-manipulated wires.

A. Elastic Rod Theory

Before the estimation of external forces and torques can occur, one would have to provide an accurate elastic rod model to compute the internal torques within the system. For our work, we have chosen to use the discrete elastic rods (DER) theory [8], which has been implemented as a plugin in MuJoCo [35]. Additionally, we estimate the material properties of the wire with a simple parameter identification pipeline [36].

IV. Formulation

The total torque on piece i of the discretized rod is

$$\tau^i_{total} - c\omega = \mathbf{I}\alpha \tag{1}$$

where $\mathbf{I}$ is the second area moment of inertia, α is the angular acceleration vector, $c\omega$ is the damping torque, and τ^i_{total} is the overall torque on piece i, excluding damping torque. When the rod is in static equilibrium, $\alpha = 0$, $c\omega = 0$.

$$\tau^i_{total} = \left(\mathbf{e}^i \times \mathbf{F}^i\right) + \left(\mathbf{a}^i \times {\mathbf{f}_\mathbf{c}}^i\right) + {\tau_c}^i + \mathbf{c}^i = 0, \tag{2}$$

where $\mathbf{F}^i = \sum_{\mathbf{f}^j \in G_i} \mathbf{f}^j$ such that G_i is the set of all external forces belonging to D sections after piece i (i.e., D sections containing pieces with index $> i$). This means that $\mathbf{F}^k = \mathbf{F}^l$ if k and l belong to the same UD section. ${\mathbf{f}_\mathbf{c}}^i$ and ${\tau_c}^i$ are respectively the external force and torque on piece i and are equal to 0 if i belongs to an UD section. $\mathbf{a}^i = \mathbf{p}_i - \mathbf{x}_i = r\mathbf{e}^i$

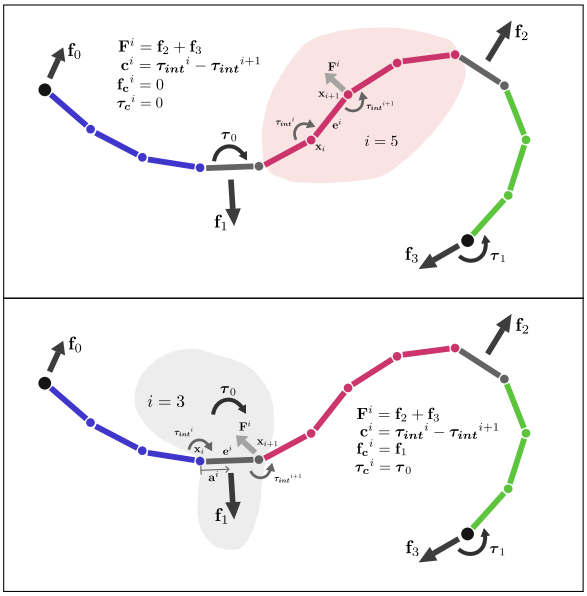

Fig. 2. Simplified 2D diagrams describing the variables used in the formulation of our method: Undisturbed (UD; top; $i = 5$) and disturbed (D; bottom; $i = 3$) sections. The color of the pieces represents: black ends - fixed nodes, grey - D pieces, other colored - UD pieces.

where $\mathbf{p}_i$ is the point of application of ${\mathbf{f}_\mathbf{c}}^i$, and $r \in [0,1] \subset \mathbb{R}$. Essentially, $\mathbf{e}^i \times \mathbf{F}^i$ is the torque induced by external forces acting on the D sections downstream of (i.e., with higher index than) piece i, and $\mathbf{a}^i \times {\mathbf{f}_\mathbf{c}}^i$ is the torque induced by external forces acting on the section that piece i belongs to. $\mathbf{c}^i = {\tau_{int}}^i - {\tau_{int}}^{i+1}$, where $\mathbf{c}^i$ is the stiffness torque applied on piece i by its adjacent pieces (not to be confused with unbold c), and ${\tau_{int}}^i$ is the internal stiffness torque applied by piece $i-1$ on i. Simplified diagrams including the variables used is shown in Figure 2.

Note that the effects of gravity are included by adding the torque effects of gravity from the side which $\mathbf{F}_R$ is acting (i.e., adding $\left((n-i-0.5)\mathbf{e}^i\right) \times \mathbf{wpp}$ to $\mathbf{c}^i$ where $\mathbf{wpp}$ is a 3-vector describing the weight per piece of the discretized wire). In favor of improved readability, the gravity term is hidden in later formulations but present in the source code and experiments.

A. Identifying Positions of Disturbances

Suppose two pieces i and $i+1$ belong to the same UD section, the following equations must be consistent.

$$\mathbf{e}^i \times \mathbf{F}^i = -\mathbf{c}^i \tag{3}$$

$$\mathbf{e}^{i+1} \times \mathbf{F}^{i+1} = -\mathbf{c}^{i+1} \tag{4}$$

Knowing $\mathbf{F}^i = \mathbf{F}^{i+1}$, we arrive at the first consistency condition (condition A) which states that $\mathbf{e}^i \cdot \mathbf{c}^{i+1} + \mathbf{e}^{i+1} \cdot \mathbf{c}^i = 0$. This is a necessary condition to conclude that these adjacent pieces belong in the same UD section. To check for sufficiency, we investigate the case of piece i belonging to an adjacent D section.

$$\mathbf{e}^i \times \mathbf{F}^i + \mathbf{a}^i \times {\mathbf{f}_\mathbf{c}}^i + {\tau_c}^i = -\mathbf{c}^i \tag{5}$$

Using triple vector product rule on (4) and (5), we get

$$\mathbf{f_c}^i \cdot \left(\mathbf{e}^{i+1} \times \mathbf{a}^i\right) + \mathbf{e}^{i+1} \cdot \tau_c{}^i = -\left(\mathbf{e}^i \cdot \mathbf{c}^{i+1} + \mathbf{e}^{i+1} \cdot \mathbf{c}^i\right). \quad (6)$$

Knowing that RHS of (6) $= 0$ and $\mathbf{e}^{i+1} \times \mathbf{a}^i \neq 0$ (non-collinearity condition), we find that the consistency condition can be fulfilled in two cases. The first is when $\mathbf{f_c}^i = 0$, which confirms that pieces i and $i+1$ belong to the same UD section. The second is when $\mathbf{f_c}^i \cdot \left(\mathbf{e}^{i+1} \times \mathbf{a}^i\right) = 0$. Since $\mathbf{a}^i \parallel \mathbf{e}^i$, this means that condition A can be fulfilled even when the two pieces belong to different sections as long as $\mathbf{f_c}^i$ lies in the plane spanned by $\mathbf{e}^i$ and $\mathbf{e}^{i+1}$, and $\tau_c{}^i \perp \mathbf{e}^{i+1}$. Therefore, condition A is not a sufficient condition.

To establish a sufficient condition for pieces to belong to the same UD section, we must check the consistency of 3 adjacent pieces.

$$\text{Given } \overset{9\times3}{\mathbf{A}_i} = \begin{bmatrix} [\mathbf{e}^i]_\times & [\mathbf{e}^{i+1}]_\times & [\mathbf{e}^{i+2}]_\times \end{bmatrix}^T \quad (7)$$

$$\text{and } \overset{9\times1}{\mathbf{C}_i} = -\begin{bmatrix} \mathbf{c}^i & \mathbf{c}^{i+1} & \mathbf{c}^{i+2} \end{bmatrix}^T, \quad (8)$$

where $[\mathbf{e}]_\times$ is the skew symmetric of 3-vector $\mathbf{e}$.

We solve for $\mathbf{F}^* = \underset{\mathbf{F}}{\operatorname{argmin}} \|\mathbf{AF} - \mathbf{C}\|_2^2$ using least squares.

$$\mathbf{F}^* = \mathbf{A}^+\mathbf{C} \quad (9)$$

where $\mathbf{A}^+ = \mathbf{V}\Sigma^+\mathbf{U}^T$ is the pseudoinverse of $\mathbf{A}$ arrived at from the singular value decomposition (SVD) of $\mathbf{A} = \mathbf{U}\Sigma\mathbf{V}^T$. The second consistency condition is evaluated by comparing the residual of the above equation ($res = \|\mathbf{AF}^* - \mathbf{C}\|_2^2$) to a manually designed threshold ($res < thres_B$). This is termed condition B – a necessary and sufficient condition to conclude that the pieces involved belong to the same UD section.

B. Estimating External Disturbances

After we have classified the discretized wire pieces into their D and UD sections, we solve for external disturbances.

1) Estimating External Forces: It is interesting to note that it is not possible to solve for forces with only one UD piece $\mathbf{e}^i \times \mathbf{F}^i = \left[\mathbf{e}^i\right]_\times \cdot \mathbf{F}^i = -\mathbf{c}^i$, as the skew-symmetric of a 3-vector is maximally rank 2, resulting in an underdetermined problem. As such a minimum of 2 pieces is required. For pieces belonging to the same UD section, the $\mathbf{F}^*$ values from the classification step are averaged to arrive at $\mathbf{F}_R$.

As the wire consists of alternating D and UD sections, the force on section D_j can be calculated as

$$\mathbf{f}^j = \mathbf{F}_R^k - \mathbf{F}_R^l + \mathbf{f}_g^j \quad (10)$$

such that k and l belong to consecutive UD sections separated by D_j, $k < l$, and $\mathbf{f}_g^j = n_{\mathrm{D}_j} \times \mathbf{wpp}$ is the force contribution due to gravity.

2) Estimating External Torques or Force Positions: The torque at each D section is determined by

$$\tau_{\mathrm{D}_j} = \left(\mathbf{e}_\mathrm{D}^j \times \mathbf{F}_\mathrm{D}^j\right) + \left(\mathbf{a}_\mathrm{D}^j \times \mathbf{f}^j\right) + \mathbf{c}_\mathrm{D}^j + \tau^j, \quad (11)$$

such that $\mathbf{e}_\mathrm{D}^j = \mathbf{x}_k - \mathbf{x}_l$ where k and l are the pieces on the two ends of section D_j and $k > l$. $\mathbf{a}_\mathrm{D}^j = \mathbf{p}_j - \mathbf{x}_l$ where $\mathbf{p}_j$ is the point of application of the external force $\mathbf{f}^j$. $\mathbf{c}_\mathrm{D}^j$ is the stiffness torque applied on D_j by the UD pieces just adjacent to section D_j (gravity contributions can be added to this term). Assuming static equilibrium, overall torque $\tau_{\mathrm{D}_j} = 0$.

The problem is indeterminate because there is only one equation with two unknowns: force position ($\mathbf{p}_j$) and external torque (τ^j).

There are three possible solutions following this. The first two solutions either use (1) a known position of external force application $\mathbf{p}_j$ or (2) assume the force is applied at the mass center of the D section ($\mathbf{p}_j = (\mathbf{x}_k - \mathbf{x}_l)/2$) to compute the external torque τ^j.

The third solution assumes that torque acting on the D section is 0 ($\tau^j = 0$) and compute the exact point of external force application $\mathbf{p}_j$ on the D section.

The results from our real-world experiments utilize the second solution ($\mathbf{p}_j = (\mathbf{x}_k - \mathbf{x}_l)/2$), as the scope of our work is limited to force prediction. Estimating torque would require capturing internal twist from RGB-D data – a problem that remains an open challenge in the field.

V. Simulation Experiments

A wire was clamped at two points 50 cm apart along the wire length, held 30 cm apart horizontally with the excess left to dangle. Perfect knowledge of wire stiffness values was assumed. The environment used an adapted DER model [36] to simulate bending and twisting behaviors and compute internal stiffness torques, with the algorithm taking only the wire's pose as input. Wire twist was captured via API, a capability unavailable in real experiments. Sample results are plotted in Figure 5, with a video available at `https://youtu.be/fAAVQuVog4Y`.

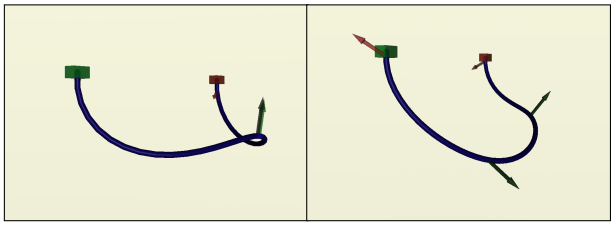

Fig. 3. Screenshots of force estimation simulation experiments. Forces are applied through the interactive user visualization window (left) or the API (right: multi-contact scenario). The actual (black) and estimated (green) forces are shown (overlapping).

Additional simulation experiments were conducted to measure computational performance. Results are plotted in Figure 4 and discussed in the following sections.

A. Computation Time vs. Number of Discrete Pieces

Solver call times were evaluated across configurations discretized into $n \in \{10, 20, 30, 50, 100, 150\}$ pieces, with two sinusoidal forces of magnitude $\frac{\sqrt{2}}{4}$N rotating in the yz-plane at 0.1 Hz, $\pi/2$ rads out of phase, applied at the one-third and two-thirds points. Each simulation ran for 20 seconds (~ 1000 function calls). Computation time increases linearly with n_{pieces} (Figure 4A), indicating that computational cost does not grow unreasonably at higher resolutions. Even at

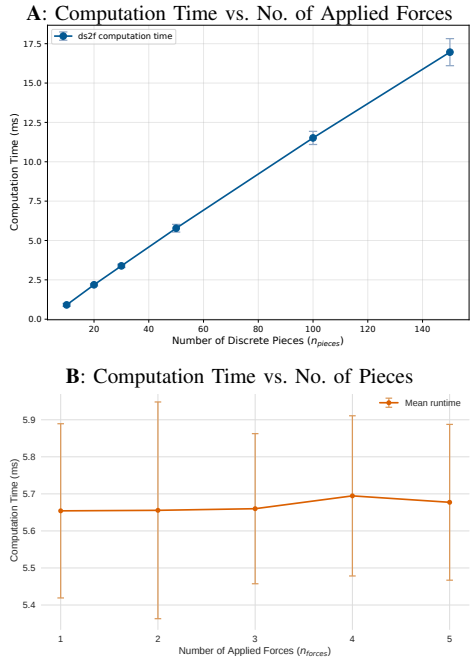

Fig. 4. Simulation experiments for computation speed against: number of pieces (**A**) and number of contacts (**B**), along with the corresponding standard deviation of results.

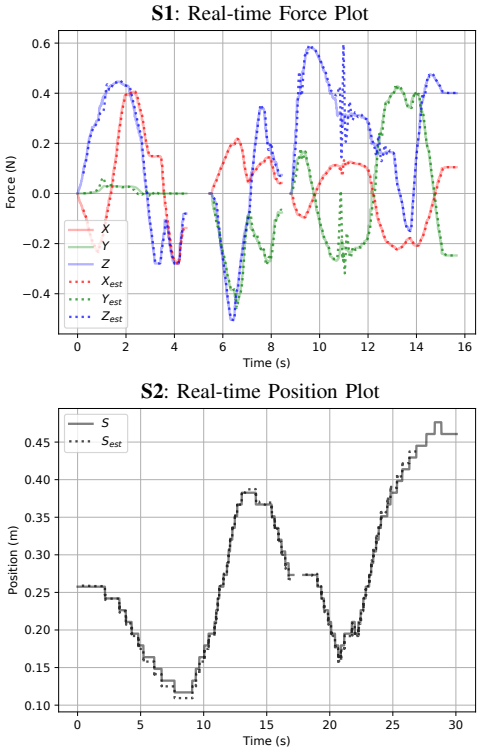

Fig. 5. Simulation experiments for force estimation. Two simulation experiments were carried out: **S1** shows the force estimation for varying force magnitude and direction on disturbances at the center of the wire length. **S2** shows the estimation of force position when the point of force application was varied. The solid and dotted lines are the actual and estimated data, respectively. Video of the experiments found here: `https://youtu.be/fAAVQuVog4Y`.

$n_{\text{pieces}} = 150$, the solver remained within practical bounds for real-time applications ($< 1/30$s).

B. Computation Time vs. Number of Contact Forces

Using a fixed discretization of $n_{\text{pieces}} = 50$, the number of simultaneously applied forces was varied across $n_{\text{forces}} \in \{1,2,3,4,5\}$, distributed evenly along the wire. Each force rotated sinusoidally at 0.1 Hz with magnitude $\frac{\sqrt{2}}{4}$N, with consecutive forces offset by $2\pi/n_{\text{forces}}$ rads. The near-constant computation time across contact counts (Figure 4B) suggests that multi-contact scenarios introduce negligible additional computational overhead.

C. Quasistatic Assumption

Force estimation performed better under less wire movement, as expected from the quasistatic assumption. Visual observations suggested reasonable stability even under significant motion, though quantitative investigation remains for future work.

VI. Physical Experiments

A. Experimental Set-up

The set-up followed the simulation experiments. A Denso VS-060 robot arm was fitted with a force-torque sensor at its end-effector along with a custom wire clamp attachment. The robot arm was used to manipulate the wire first at its midpoint and then at a 7 cm offset along the wire length from its center. Actual force readings were recorded with the force-torque sensor and filtered using a Chebyshev filter. Due to the limitation of capturing internal twist from visual and depth information, our results assumed a zero-twist configuration of the rod, focusing solely on force prediction and not torque estimation. Although gripper movement would introduce external torque on the wire, this did not affect force prediction, as the force prediction and torque estimation parts of the pipeline were separate. The result was still a prediction of the external force from the gripper on the wire.

The wire shape was obtained through the pipeline presented in [37], leveraging GROUNDED-SAM, a zero-shot image segmentation framework, which we found to be both easy to implement and accurate, with the drawback of longer computational times (overall detection pipeline takes 8 s per 720p frame on an NVIDIA GeForce RTX 3060 Ti GPU). The wire was discretized into 60 pieces after smoothing and interpolated into 30 discrete pieces for further processing. For DLO smoothing, we used a trade-off between the error from node displacement due to smoothing (p_{smooth}) and the decrease in elastic potential energy in the rod (E_{decrease}). As long as $J_i > J_{i-1}$ where i is the time step and $J = E_{\text{decrease}} - m_p * p_{\text{smooth}}$, smoothing continued. In this work, we applied time stepping through the DER model implemented in MuJoCo and included a plugin state which provides the potential energy in the rod. The same model was used to compute internal torques in the rod.

B. Results

The experiments were split into two main parts. Coordinate frame of the experiment was defined as shown in plots

of Figure 6. For the first part (**A**), the wire was clamped to the robot end-effector at its center (25 cm along its length from the left end) in its equilibrium position and moved into 6 different positions with pure translational motion (orientation remains constant). Position displacement from the neutral positions are shown in Figure 6. These positions were selected for variety and the distance was chosen to ensure the condition of non-parallel discrete pieces was fulfilled as much as possible (to avoid an underdetermined problem). The actual and estimated force vectors for experiment **A** are shown in Figure 6. Vectors within each plot are shown to scale relative to each other, but their scales are not consistent across different plots.

For the second part (**B**), the wire was clamped to the robot end-effector at a 7 cm offset along the wire length from its center (18 cm along its length from the left end) in its equilibrium position and moved into 4 different positions with pure translational motion. The actual and estimated force vectors for experiment **B** are shown in Figure 7. Overall quantitative results for both experiments (**A** and **B**) comparing the actual ($\mathbf{F}_{\text{act}}$) and estimated ($\mathbf{F}_{\text{est}}$) forces are shown in Table I. To evaluate the accuracy of the estimated force $\mathbf{F}_{\text{est}}$ compared to the actual force $\mathbf{F}_{\text{act}}$, we computed several error metrics. To assess directional accuracy, we computed the *angle difference* between the vectors. The *relative L2 error* normalizes the L2 error by the magnitude of the actual force, yielding $\frac{\|\mathbf{F}_{\text{est}}-\mathbf{F}_{\text{act}}\|_2}{\|\mathbf{F}_{\text{act}}\|_2+\varepsilon}$, where ε is a small constant added to avoid division by zero. Lastly, to evaluate the spatial accuracy of the estimated point of application, we computed the *position difference* between the estimated and actual contact points as $\|\mathbf{p}_{\text{est}}-\mathbf{p}_{\text{act}}\|_2$, where $\mathbf{p}$ is the position at which the force acts.

TABLE I
QUANTITATIVE RESULTS COMPARISON FOR FORCE ESTIMATION

Experiment	Relative L2 Err. (N)	Angle Diff. (°)	Position Diff. (mm)
A1	0.2521	0.2225	8.242
A2	0.1364	0.1176	0.0006
A3	0.1522	0.1452	24.93
A4	0.8009	0.8887	8.278
A5	0.6218	0.2091	8.422
A6	0.4223	0.0367	32.31
B1	1.0491	1.1323	33.45
B2	0.1281	0.1103	33.32
B3	0.4021	0.4133	7.494
B4	0.9419	0.9235	30.67

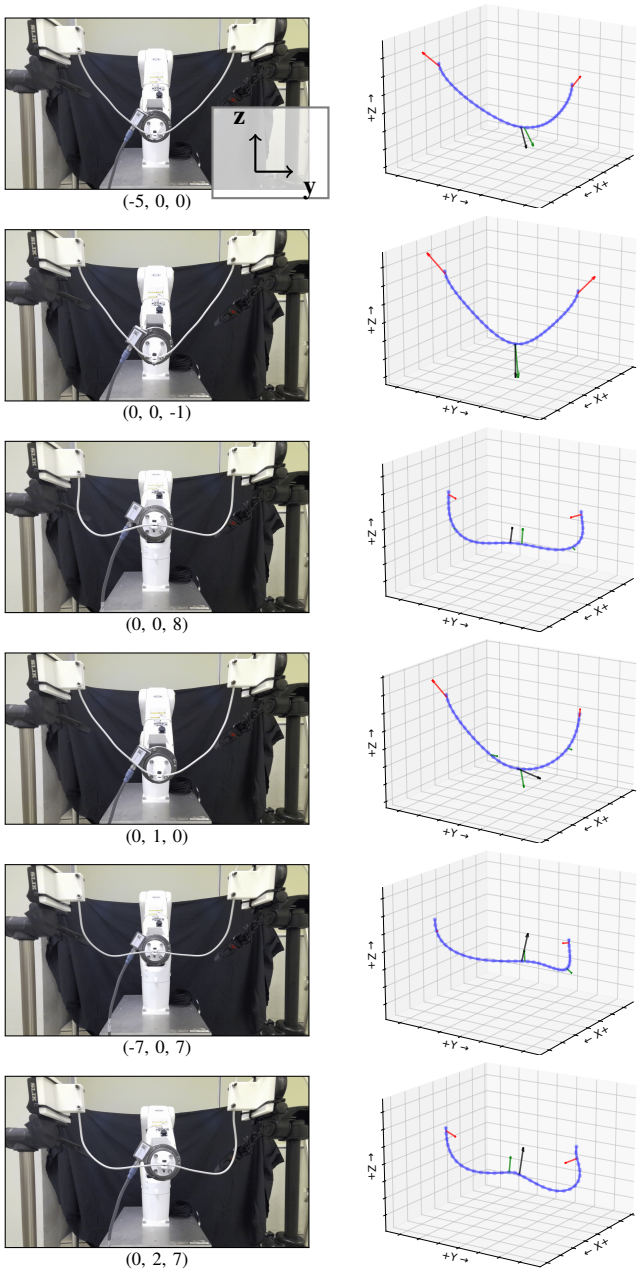

Fig. 6. Visual results of force estimation for experiment **A** where the wire was clamped at both ends and attached to the robot end-effector at its center. The robot end-effector was fitted with a force-torque sensor and moved into 6 different positions. The left column shows the real experiment images (coordinates axes shown in first image) with Cartesian displacement of the grasped point (below), and the right column shows the smoothed wire shape along with the actual and estimated force vector (arrows: red - estimated end-clamp force, black - actual force, green - estimated external force). Note that the accuracy of end-clamp forces are not analyzed.

C. Discussion

In scenarios **A4**, **A5**, **B1**, and **B4**, additional erroneous forces were detected. For our analysis, we only compared the largest magnitude force with the actual force sensed. The *relative L2 error* and *angle difference* were generally lower for single direction wire displacements, with the exception of **B1**. Along with **A4**, **A6**, and **B4**, we found that displacement and forces in the x-direction were not easily detected with our method and caused larger relative L2 errors and angle differences. For the cases of **A4** and **B4**, the algorithm

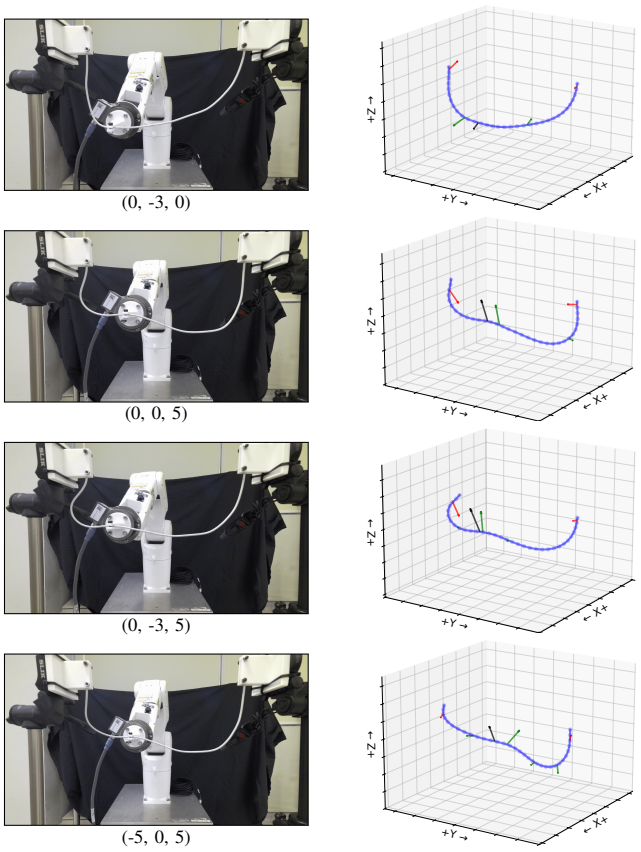

Fig. 7. Visual results of force estimation for experiment **B** where the wire was clamped at both ends and attached to the robot end-effector at a 7 cm offset along the wire length from its center.

seemed to dissect the forces and identify additional force disturbances (other green arrows) which have an x-direction contribution, but these were not considered in our analysis.

Interestingly, these forces which were difficult to detect were those that act nearly tangentially to the wire. That could be a hint that the algorithm in its current state is not suited to accurately determine tangential forces due to its sensitivity to pose error of the wire, and the wire physical properties. This is in agreement with previous works which assumed normal external forces to deal with high axial stiffness [32].

We speculate that force estimation errors likely result from two main causes: the wire not having purely elastic deformation properties and imperfect determination of wire position using the depth camera. The latter can be solved with improved detection capabilities. The former proves to be a more complex issue and could directly affect our results as the algorithm might recognize internal torque in the wire where it is not actually present, requiring further intense investigations into modeling of plastic deformations in DLOs.

Estimations on the position of force application were all below 40 mm and yielded better results for experiment **A** than **B**. This could be due to a displacement at the midpoint of the wire **A** producing more deformation in the wire which the algorithm is sensitive to.

Although the experiments are conducted with wires arranged in a U-shape configuration to facilitate detection and intuitive visualization, the proposed method generalizes to arbitrary wire shapes and grasp configurations, subject to the conditions outlined in Section III. Furthermore, while force estimation accuracy is evaluated only at the end-effector, the forces at both ends of the DLO are also estimated by the model. To further validate the effectiveness of the proposed pipeline in multi-contact scenarios, force sensors can be installed at the two fixed ends to quantitatively assess the estimated forces.

VII. Conclusion

In this work, we introduced an algorithm to estimate external forces acting on an elastic rod based on its observed shape. By deriving consistency conditions from static force-torque balance equations, we identified undisturbed sections of the rod where no external interactions occur. Leveraging this classification and internal stiffness torque models from the DER formulation, we solved for the direction and magnitude of external forces. Simulation experiments were conducted to characterize the solver's computational scaling with discretization resolution and number of simultaneous contacts. Results of physical experiments validated the method's effectiveness by comparing the estimated forces against ground truth readings from physical sensors during robot-wire interactions.

A. Limitations and Future Work

Throughout our experiments, we assume the wire behaves in a purely elastic manner. Plasticity and potential hysteresis in real wires affect the predicted forces. Future work can utilize model-based [38] and model-free [39], [40] approaches to incorporate plasticity and uncertainty into the model.

Currently, the wire detection pipeline uses an Azure Kinect RGB-D camera along with a zero-shot image segmentation model. This approach is potentially slow and noisy. Future work could incorporate faster and more robust detection pipelines to enable more precise wire state estimation, which is critical to the success of our proposed method. This remains an active area of research within the field of deformable linear object perception [37], [41]–[44].

Future work can study the sensitivity of our method to position and parameter errors, and the effects of violating the quasistatic condition. Further investigation could also assess the pipeline's robustness to rotational disturbances and more contacts.

References

[1] A. Schlechter and D. Henrich, "Manipulating deformable linear objects: Characteristics in force signals for detecting contact state transitions," 2001.

[2] A. X. Lee, H. Lu, A. Gupta, S. Levine, and P. Abbeel, "Learning force-based manipulation of deformable objects from multiple demonstrations," in *2015 IEEE International Conference on Robotics and Automation (ICRA)*. IEEE, 2015, pp. 177–184.

[3] N. Nakagawa and H. Mochiyama, "Real-time shape estimation of an elastic rod using a robot manipulator equipped with a sense of force," in *2018 IEEE/RSJ International Conference on Intelligent Robots and Systems (IROS)*. IEEE, 2018, pp. 8067–8073.

[4] F. Süberkrüb, R. Laezza, and Y. Karayiannidis, "Feel the tension: Manipulation of deformable linear objects in environments with fixtures using force information," in *2022 IEEE/RSJ International Conference on Intelligent Robots and Systems (IROS)*. IEEE, 2022, pp. 11 216–11 222.

[5] H. Zhong, Z. Xu, G. Ma, M. Yu, and X. Li, "Regressor-based model adaptation for shaping deformable linear objects with force control," in *2023 IEEE International Conference on Robotics and Biomimetics (ROBIO)*. IEEE, 2023, pp. 1–7.

[6] H. G. Nguyen, M. Kuhn, and J. Franke, "Manufacturing automation for automotive wiring harnesses," *Procedia Cirp*, vol. 97, pp. 379–384, 2021.

[7] K. J. Wessel, I. Wendenburg, C. Varnava, S. Wellenbrock, A. Dermietzel, M. Hiort, D. Kampshoff, P. Wiebringhaus, T. Hirsch, and M. Kueckelhaus, "Ideal suturing technique for robot-assisted microsurgical anastomoses," *Journal of Robotic Surgery*, vol. 18, no. 1, p. 272, 2024.

[8] M. Bergou, M. Wardetzky, S. Robinson, B. Audoly, and E. Grinspun, "Discrete elastic rods," in *ACM SIGGRAPH 2008 papers*, 2008, pp. 1–12.

[9] A. Wahrburg, J. Bös, K. D. Listmann, F. Dai, B. Matthias, and H. Ding, "Motor-current-based estimation of cartesian contact forces and torques for robotic manipulators and its application to force control," *IEEE Transactions on Automation Science and Engineering*, vol. 15, no. 2, pp. 879–886, 2017.

[10] G. Wang, Z. Wang, B. Huang, Y. Gan, and F. Min, "Active compliance control based on ekf torque fusion for robot manipulators," *IEEE Robotics and Automation Letters*, vol. 8, no. 5, pp. 2668–2675, 2023.

[11] S. Shan and Q.-C. Pham, "Fine robotic manipulation without force/torque sensor," *IEEE Robotics and Automation Letters*, vol. 9, no. 2, pp. 1206–1213, 2023.

[12] T. Bretl and Z. McCarthy, "Quasi-static manipulation of a kirchhoff elastic rod based on a geometric analysis of equilibrium configurations," *The International Journal of Robotics Research*, vol. 33, no. 1, pp. 48–68, 2014.

[13] A. Borum and T. Bretl, "The free configuration space of a kirchhoff elastic rod is path-connected," in *2015 IEEE International Conference on Robotics and Automation (ICRA)*. IEEE, 2015, pp. 2958–2964.

[14] R. Takano, H. Mochiyama, and N. Takesue, "Real-time shape estimation of kirchhoff elastic rod based on force/torque sensor," in *2017 IEEE International Conference on Robotics and Automation (ICRA)*. IEEE, 2017, pp. 2508–2515.

[15] J. L. Novak and J. T. Feddema, "A capacitance-based proximity sensor for whole arm obstacle avoidance," Sandia National Labs., Albuquerque, NM (United States), Tech. Rep., 1991.

[16] A. Albini, F. Grella, P. Maiolino, and G. Cannata, "Exploiting distributed tactile sensors to drive a robot arm through obstacles," *IEEE Robotics and Automation Letters*, vol. 6, no. 3, pp. 4361–4368, 2021.

[17] K. Nuelle, M.-J. Schulz, S. Aden, A. Dick, B. Munske, J. Gaa, J. Kotlarski, and T. Ortmaier, "Force sensing, low-cost manipulator in mobile robotics," in *2017 3rd International Conference on Control, Automation and Robotics (ICCAR)*. IEEE, 2017, pp. 196–201.

[18] A. De Luca and R. Mattone, "Sensorless robot collision detection and hybrid force/motion control," in *Proceedings of the 2005 IEEE international conference on robotics and automation*. IEEE, 2005, pp. 999–1004.

[19] S. Haddadin, A. Albu-Schaffer, A. De Luca, and G. Hirzinger, "Collision detection and reaction: A contribution to safe physical human-robot interaction," in *2008 IEEE/RSJ International Conference on Intelligent Robots and Systems*. IEEE, 2008, pp. 3356–3363.

[20] C.-N. Cho, J.-H. Kim, S.-D. Lee, and J.-B. Song, "Collision detection and reaction on 7 dof service robot arm using residual observer," *Journal of mechanical science and technology*, vol. 26, no. 4, pp. 1197–1203, 2012.

[21] S. Haddadin, A. De Luca, and A. Albu-Schäffer, "Robot collisions: A survey on detection, isolation, and identification," *IEEE Transactions on Robotics*, vol. 33, no. 6, pp. 1292–1312, 2017.

[22] L. D. Phong, J. Choi, and S. Kang, "External force estimation using joint torque sensors for a robot manipulator," in *2012 IEEE International Conference on Robotics and Automation*, 2012, pp. 4507–4512.

[23] D.-H. Lee, W. Hwang, and S.-C. Lim, "Interaction force estimation using camera and electrical current without force/torque sensor," *IEEE Sensors Journal*, vol. 18, no. 21, pp. 8863–8872, 2018.

[24] C. Gaz and A. De Luca, "Payload estimation based on identified coefficients of robot dynamics—with an application to collision detection," in *2017 IEEE/RSJ International Conference on Intelligent Robots and Systems (IROS)*. IEEE, 2017, pp. 3033–3040.

[25] S. Shan and Q.-C. Pham, "Fast payload calibration for sensorless contact estimation using model pre-training," *IEEE Robotics and Automation Letters*, 2024.

[26] L. Han, W. Xu, B. Li, and P. Kang, "Collision detection and coordinated compliance control for a dual-arm robot without force/torque sensing based on momentum observer," *IEEE/ASME Transactions on Mechatronics*, vol. 24, no. 5, pp. 2261–2272, 2019.

[27] L. Manuelli and R. Tedrake, "Localizing external contact using proprioceptive sensors: The contact particle filter," in *2016 IEEE/RSJ International Conference on Intelligent Robots and Systems (IROS)*. IEEE, 2016, pp. 5062–5069.

[28] T. Pang, J. Umenberger, and R. Tedrake, "Identifying external contacts from joint torque measurements on serial robotic arms and its limitations," in *2021 IEEE International Conference on Robotics and Automation (ICRA)*. IEEE, 2021, pp. 6476–6482.

[29] E. Magrini and A. De Luca, "Human-robot coexistence and contact handling with redundant robots," in *2017 IEEE/RSJ International Conference on Intelligent Robots and Systems (IROS)*. IEEE, 2017, pp. 4611–4617.

[30] J. Back, T. Manwell, R. Karim, K. Rhode, K. Althoefer, and H. Liu, "Catheter contact force estimation from shape detection using a real-time cosserat rod model," in *2015 IEEE/RSJ International Conference on Intelligent Robots and Systems (IROS)*. IEEE, 2015, pp. 2037–2042.

[31] V. A. Aloi and D. C. Rucker, "Estimating loads along elastic rods," in *2019 International Conference on Robotics and Automation (ICRA)*. IEEE, 2019, pp. 2867–2873.

[32] V. Aloi, K. T. Dang, E. J. Barth, and C. Rucker, "Estimating forces along continuum robots," *IEEE Robotics and Automation Letters*, vol. 7, no. 4, pp. 8877–8884, 2022.

[33] S. Lilge, T. Barfoot, and J. Burgner-Kahrs, "State estimation for continuum multirobot systems on se (3)," *IEEE Transactions on Robotics*, vol. 41, pp. 905–925, 2024.

[34] J. M. Ferguson, D. C. Rucker, and R. J. Webster, "Unified shape and external load state estimation for continuum robots," *IEEE Transactions on Robotics*, vol. 40, pp. 1813–1827, 2024.

[35] E. Todorov, T. Erez, and Y. Tassa, "Mujoco: A physics engine for model-based control," in *2012 IEEE/RSJ international conference on intelligent robots and systems*. IEEE, 2012, pp. 5026–5033.

[36] Q. J. Chen, T. Bretl, and Q.-C. Pham, "Accurate simulation and parameter identification of deformable linear objects using discrete elastic rods in generalized coordinates," in *2025 IEEE/RSJ International Conference on Intelligent Robots and Systems (IROS)*. IEEE, 2025, pp. 20 454–20 460.

[37] S. Zhaole, H. Zhou, L. Nanbo, L. Chen, J. Zhu, and R. B. Fisher, "A robust deformable linear object perception pipeline in 3d: From segmentation to reconstruction," *IEEE Robotics and Automation Letters*, vol. 9, no. 1, pp. 843–850, 2023.

[38] D. Terzopoulos and K. Fleischer, "Deformable models," *The visual computer*, vol. 4, no. 6, pp. 306–331, 1988.

[39] R. Laezza and Y. Karayiannidis, "Learning shape control of elastoplastic deformable linear objects," in *2021 IEEE International Conference on Robotics and Automation (ICRA)*. IEEE, 2021, pp. 4438–4444.

[40] C. Matl and R. Bajcsy, "Deformable elasto-plastic object shaping using an elastic hand and model-based reinforcement learning," in *2021 IEEE/RSJ International Conference on Intelligent Robots and Systems (IROS)*. IEEE, 2021, pp. 3955–3962.

[41] A. Caporali and G. Palli, "Robotic manipulation of deformable linear objects via multiview model-based visual tracking," *IEEE/ASME Transactions on Mechatronics*, 2025.

[42] A. Caporali, K. Galassi, B. L. Žagar, R. Zanella, G. Palli, and A. C. Knoll, "Rt-dlo: Real-time deformable linear objects instance segmentation," *IEEE Transactions on Industrial Informatics*, vol. 19, no. 11, pp. 11 333–11 342, 2023.

[43] J. Xiang, H. Dinkel, H. Zhao, N. Gao, B. Coltin, T. Smith, and T. Bretl, "Trackdlo: Tracking deformable linear objects under occlusion with motion coherence," *IEEE Robotics and Automation Letters*, vol. 8, no. 10, pp. 6179–6186, 2023.

[44] K. Lv, M. Yu, Y. Pu, X. Jiang, G. Huang, and X. Li, "Learning to estimate 3-d states of deformable linear objects from single-frame occluded point clouds," *arXiv preprint arXiv:2210.01433*, 2022.